Results in Physics 7 (2017) 777–788

Contents lists available at ScienceDirect

Results in Physics

journal homepage: www.journals.elsevier.com/results-in-physics

# Investigation of microstructural and physical characteristics of nano composite tin oxide-doped $Al^{3+}$ in $Zn^{2+}$ based composite coating by DAECD technique

P.A.L. Anawe [a], O.S.I. Fayomi [b,c,*], A.P.I. Popoola [b]

[a] Department of Petroleum Engineering, Covenant University, P.M.B 1023, Ota, Nigeria
[b] Department of Chemical, Metallurgical and Materials Engineering, Tshwane University of Technology, P.M.B. X680, Pretoria, South Africa
[c] Department of Mechanical Engineering, Covenant University, P.M.B 1023, Ota, Nigeria

ARTICLE INFO

*Article history:*
Received 13 January 2017
Received in revised form 24 January 2017
Accepted 24 January 2017
Available online 30 January 2017

*Keywords:*
Microstructure
Wear
Composite
Microhardness
Deposit

ABSTRACT

In other to overcome the devastating deterioration of mild steel in service, Zn-based embedded Al/$SnO_2$ composite coatings have been considered as reinforcing alternative replacements to the more traditional deposition for improved surface properties by using Dual Anode Electrolytic Co-deposition (DAECD) technique from chloride bath. The structural characterization of the starting materials and deposited coating are evaluated using scanning electron microscopy (SEM), equipped with energy dispersive X-ray spectroscopy (EDX) elemental analysis and atomic force microscope (AFM). The hardness behaviour, wear and intermetallic distribution was examined by diamond based microhardness tester, CETR reciprocating sliding test rig and X-ray diffractometer (XRD) respectively. The corrosion properties of the developed coating were examined in 3.5% NaCl. The microstructure of the deposited sample obtained at 7% $SnO_2$, revealed fine-grains deposit of the Al/$SnO_2$ on the mild steel surface. The results showed that the Al/$SnO_2$ strengthening alloy plays a significant role in impelling the wear and corrosion behaviour of Zn-Al/$SnO_2$ coatings in an aggressive saline environment. Interestingly Zn-30Al-7Sn-chloride showed the highest wear and improved corrosion resistance due to Al/$SnO_2$ oxide passive film that forms during anodic polarization. This work established that co-deposition of mild steel with Al/$SnO_2$ is auspicious in increasing the anti-wear and corrosion progression.



## Introduction

The severe consequences of corrosion degradation and mechanical fallout have become a problem of worldwide significance [1–4]. Corrosion is an electrochemical occurrence; it is the destructive mortification of a metal and alloy by chemical or electrochemical activities by its environment [5,6]. Corrosion control is achieved by recognizing and understanding corrosion mechanisms, by using corrosion-resistant materials and designs, and by using protective systems, devices, and treatments [7–9]. The effects of corrosion failures on the performance and maintenance of materials would often be minimized if life monitoring and control of the environmental and human factors supplemented efficient designs. One of the key factors in any corrosion situation is the environment to surface reaction of materials [10]. Variables such as time, humidity and temperature instigate corrosion occurrences in major environments [11].

It is also important to realize that the environment that actually affects a metal corresponds to the micro environmental conditions and macro-mechanical properties that this metal really "sees" that is the local environment at the surface of the metal. It is indeed the reactivity of this local environment that determines the real corrosion and tribological damage [12,13]. Basically, the impure and heterogeneous nature of some metals contributes immensely to the major cause of their poor corrosion and wear resistance. In term of corrosion occurrence, the existence of anodic and cathodic sites on the metal surface and their reactivity with oxygen and water accelerate change of a metal atom to a metal ion by the loss of electrons which is also known as electrochemical corrosion [14]. Basically for mechanical challenge the structural and protective coating influence the nature of prevention [15,16].

Protective coatings are perhaps the most extensively used system for corrosion and mechanical damage control. They are used

* Corresponding author at: Department of Mechanical Engineering, Covenant University, P.M.B 1023, Ota, Nigeria.
*E-mail addresses:* ojo.fayomi@covenantuniversity.edu.ng, fayomio@tut.ac.za, ojosundayfayomi3@gmail.com (O.S.I. Fayomi), popoolaapi@tut.ac.za (A.P.I. Popoola).

http://dx.doi.org/10.1016/j.rinp.2017.01.035
2211-3797/

to provide long-term protection under a broad range of corrosive and anti-wear environments, ranging from atmospheric contact to the most demanding chemical processing conditions [17]. Protective coatings in themselves provide little or no structural strength, yet they protect other materials to preserve their strength and integrity [17–19]. The quality of a coating depends on many factors besides the nature of the materials involved, the process parameter such as the control of the pH, the stirring rate, the distance between the anode and cathode, the nature of induced bath formulation (chloride/sulphate bath) and many more. Coating and metal finishing operations are intended to increase corrosion or abrasion resistance, alter appearance, serve as an improved base for the adhesion of other materials, enhance wear and frictional characteristics, add hardness and improve electrical properties [20–22].

Composite characteristics are influenced by the deposition parameters and these have significant effect on the surface modification properties which has been reported by various authors [23–25]. Electro-codeposition route has been explored with the help of different composite additive in a single series for mild steel improvement in the past [26]. The goal of the present work is to develop a functional bath with operational zinc-rich thin film deposited in the presence of aluminum, and tin oxide and compare the bath effectiveness in relationship to process parameter on voltage and particle loading in chloride processing. However, the target is aimed at improving corrosion, mechanical and tribological properties of mild steel. This is because the roles of composites in engineering practices especially coating application in recent time are enormous.

## Materials and method

### *Materials*

A flat plate mild steel (20 mm × 20 mm × 2 mm) substrate was used in this study. The Spectrochemical analysis was indicated in Table 1. Other materials employed for the purpose of this work include pure zinc plate anode, Zinc chloride, Glycine, Thiourea, Al (45 nm, 97%purity) and Tin IV oxide (25 nm, 99.7%purity) was purchased from Sigma, South Africa.

### *Method*

#### *Sample preparation*

The mild steel plate was sectioned using automatic struers high precision cut-off machine which is connected to lubricant supply to cool the blade and sample during the cutting process. The mild steel plate was cut into equal plates of about five samples with dimensions of 20 mm by 20 mm by 2 mm.

#### *Electro-deposition*

The mild steel sample was dipped into 1 M of HCl solution for 10 s followed by rinsing into the de-ionised water. Analytical grade chemicals and de-ionised water were used to prepare the plating solutions at 40 °C, to easily dissociate any agglomerate in the bath. During the plating, the solution were stirred using the magnetic stirrer for the solution to plate well on the mild steel. The bath compositions admixed for the coatings are shown in Table 2 and they were prepared two weeks before the plating. Boric acid was added to obtain a pH of 4.8. An innovative Static current electrodeposition was used to produce Zn-Al-$SnO_2$ coating. A current density of 0.5 A/$cm^2$ was used for the deposition. The rinsing was done in distilled water for 5 s then later air dried. Table 2 shows the bath process formulation.

**Table 2**
Summarized Bath Formulation.

| Composition | Mass Concentration (g/L) |
|---|---|
| Zn | 75 |
| Al | 30 |
| KCl | 50 |
| Boric Acid | 10 |
| $SnO_2$ | 7 g–13 g |
| ZnCl | 75 |
| pH | 4.8 |
| Voltage | 0.3–0.5 V |
| Time | 20 min |
| Temp. | 40 °C |

#### *Characterization of the Electrodeposited samples*

The X-ray diffraction (XRD) patterns of the samples were obtained with an X PertPro PANalytical, LR 39487C. XRD diffractometer using Cu Kα radiation (40 kV, 40 mA). Stepwise increase for small angle was 0.01° over the range of 1–8° and wide angle rate of 1° 2θ min-1 over the range of 8–90° (2 θ). The microstructures of the samples were examined by TESCAN VEGA 3 scanning electron microscopy. Emco-test micro-hardness tester machine was used in determining the hardness values of the samples. Indentation of five points and 15 s dwell with 100 g load were used in this work.

#### *Electrochemical test*

The samples were embedded in epoxy resin leaving a working area of 0.785 $cm^2$. The control sample surface was ground with grinding papers from 600 to 1000 grit, cleaned with distilled water and ethanol. A conventional three electrode cell consisting of Platinum as counter electrode, the coated mild steel as working electrode and Ag/AgCl electrode as reference electrode respectively were used. The electrochemical measurement was done with Autolab PGSTAT 101 Metrohm potentiostat/galvanostat. An electrolytic cell containing 50 ml of 3.65% NaCl solutions as simulated solution were used as medium. The potentiodynamic potential scan was fixed from −1.5 V to +1.5 mV with scan rate of 0.012 V/s. The electrochemical corrosion test was performed at room temperature in a static solution.

#### *Reciprocating wear test*

Reciprocating ball-on-flat sliding wear tests were performed on a (CETR UMT-2) tribometer. For sliding wear tests, a 20 × 20 mm coated mild steel substrate was cut and alumina ball of 10 mm diameter was engaged as the counterface. The tests were performed under a load of 5 N with a distance of 2000 m, oscillating frequency of 5 Hz, and wear stroke length of 2 mm. The tests were carried in both dry sliding conditions. All tests were carried out at room temperature. The average wear depths of the samples at the end were used to evaluate the dry sliding wear performance. The schematic illustration of (CETR UMT-2) tribometer used is illustrated in Fig. 1.

**Table 1**
Chemical Composition of As-received Mild Steel.

| Element | C | Mn | Si | P | S | Al | Ni | Fe |
|---|---|---|---|---|---|---|---|---|
| Composition | 0.15 | 0.45 | 0.18 | 0.01 | 0.031 | 0.005 | 0.008 | 99.166 |

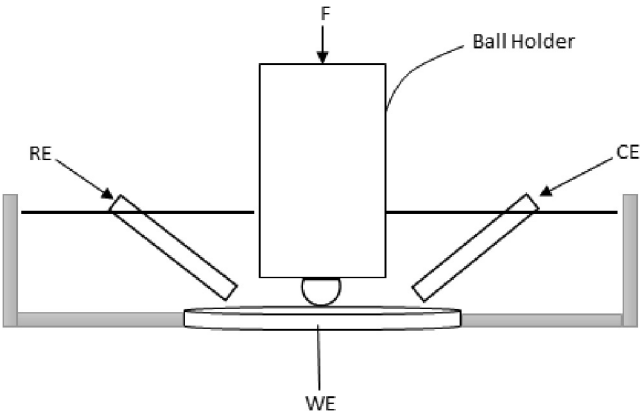


**Fig. 1.** Schematic diagram of CETR UMT-2 reciprocating sliding wear.

## Results and discussion

*Structural Characterization of the substrate and starting materials*

The substrate metal used in this study is mild steel. From the steel elemental evaluation, iron has major constituent of over 99% with carbon content approximately 0.15% among other visible elements in attendance. The average over all percentage of other metal is at minute quantity. The SEM morphology of the working steel is shown in Fig. 2 with clearly prepared surface appearance. EDS analysis also confirmed the chemical composition with Fe being the predominant element present. The phase observed from X-ray diffractograph quantification indicates specifically the presence of Fe as predominant metal (see Fig. 3). The large protrusion emerge at 2θ angles of 30–50° at 5000 count series. This shows that the as-received sample contains primarily Fe.

The nature of thin film produced is thus a function of particle induced and the purity of the base particles. Fig. 4a–c shows SEM micrographs of the particles which were used for the bath formation. The morphologies of the particles especially for zinc metal which was the base particulate were regular. This is indeed necessary reason been that dispersion effect from incorporated composite materials need regular base particle to promote adsorption and perfect precipitation on working substrate. Aluminum appearance is dull gray in nature with nonmagnetic properties; the embedded particulate will strengthen the strong bond during electrodeposition. The unadulterated and free from impurity nature of the particulate will also enhanced the flow and the loading effect of the bath produced. Tin oxide contains a high purity submicron white powdery solid with anhydride appearance. Its lightweight morphological texture will strengthen the thermal stability especially in ceramics application.

The composition of the basic chloride bath used for the preparation of ternary composite alloy coatings and the results obtained thereafter is given in Table 3. The coatings thickness and weight gain of the deposited coating were observed with inspection kit and the results were presented below.

The influence of the solid composite particles was found to be significant on the zinc interface as this maximally affect the physical properties in term of coating thickness and weight gain. At fixed time of deposition and varied potential from 0.3 to 0.5 V for 7 g, the weight gain at higher applied voltage of 0.5 V was favoured with 0.7425 g as when compared to 0.3 V with 0.2437 g. The coating thickness also increased better beyond the deposited alloy at 0.3 V. It could be seen that the resulting composite plating thickness varied linearly with fixed plating time at varied potential. The same progression was observed for the coating per unit area. Obviously, the distribution of the particulates and its coherent precipitation within the intermediate is typically influenced by the applied potential. Thus the surface properties in this case are expected to alter based on the difference in the adsorption of the particles.

To know the effect of particles as it relates to the potential involved, the composites particle concentration volumes were increased from 7 g to 13 g and potential varied accordingly. As the concentration of the additive increases in the plating bath the thickness and the weight gain values decreased this is due to the fact that increased number of the active sites are blocked hence reducing the active surface area [6]. The weight gain and coating thickness increased for 0.5 V deposited alloy at the same induced particle conditions from 0.5947 g of 0.3 V to 0.6186 g of 0.5 V. Reduced particle influence in the bath could be observed to subsequently favor 0.5 V deposits. One vital reason for this in co-deposition is that $Me^{2+}$ are adsorbed during cathodic activities with the help of hydroxide ions leading to the formation of $MeOH_{ads}$ and paving way after reduction for particle entrapment.

*Microstructural characteristics of the coating*

*Atomic force microscopy*

Figs. 5 and 6 shows typical AFM images of as-deposited Zn-Al-$SnO_2$ chloride structures and its composite variations in Zn-Al-7Sn-Cl-0.3 V and Zn-Al-13Sn-Cl-0.3 V thin film alloys respectively. The growth and topography of the coating at Zn-Al-7Sn-Cl-0.3 V

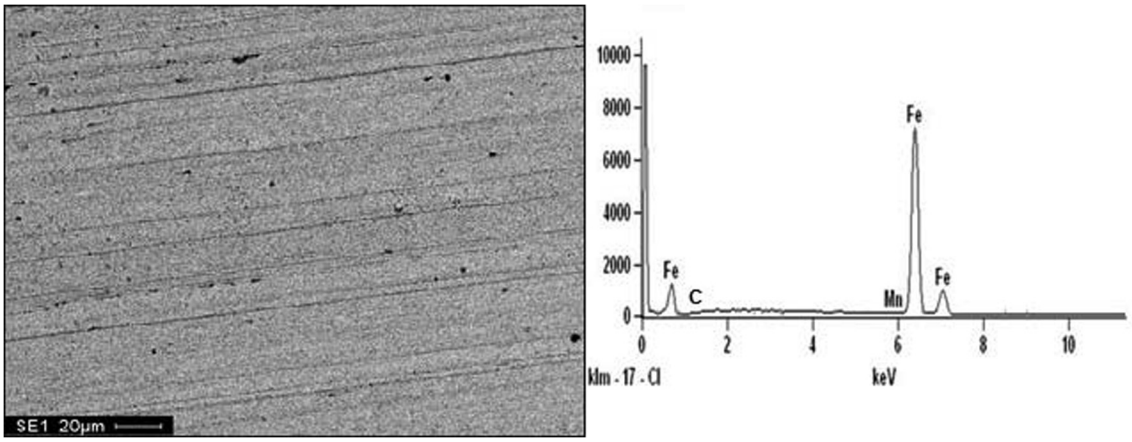


**Fig. 2.** SEM/EDS Morphology of As-received Mild Steel.

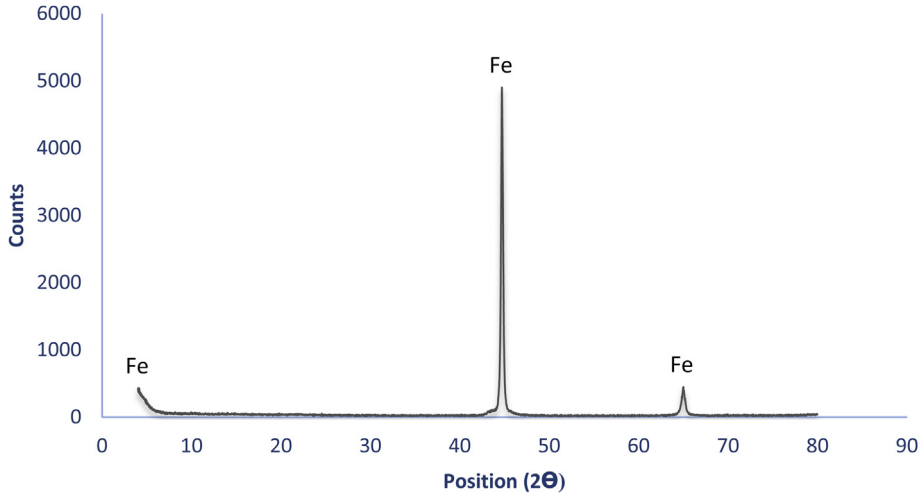


**Fig. 3.** XRD Spectrum of As-received Mild Steel.

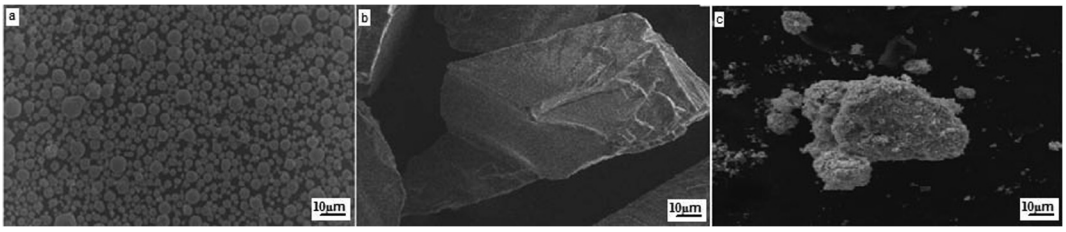


**Fig. 4.** SEM micrograph of the starting materials: (a) Zn Particle; (b) Al Particle; (c) Sn Composite.

**Table 3**
Electrodeposition Parameters and Results for Zn-Al-Sn-Cl Deposition.

| Sample | Time (min) | Coating Thickness (μm) | Weight Gain (g) | Voltage (V) | Additive Concentration (g) |
|---|---|---|---|---|---|
| Zn-Al-Sn-Cl | 20 | 141.9 | 0.2437 | 0.3 | 7 |
| Zn-Al-Sn-Cl | 20 | 150.4 | 0.7425 | 0.5 | 7 |
| Zn-Al-Sn-Cl | 20 | 133.7 | 0.5947 | 0.3 | 13 |
| Zn-Al-Sn-Cl | 20 | 110.2 | 0.6186 | 0.5 | 13 |

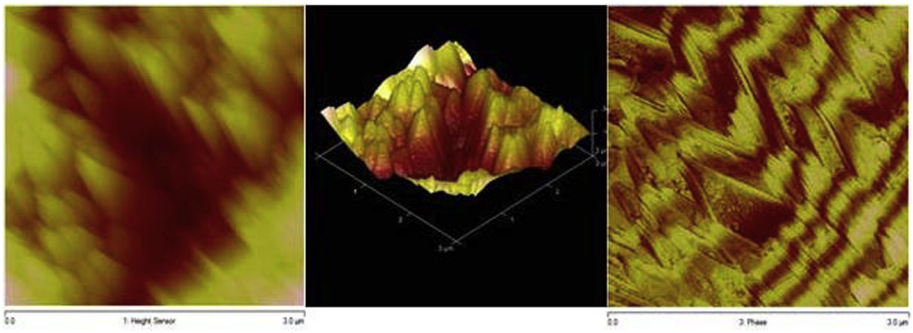

**Fig. 5.** AFM Images of the Zn-Al-7Sn-Cl-0.3 V Film: (a) 2-D image; (b) 3-D Relief Image and (c) Roughness Analysis.

demonstrate an enhanced uniform and good distribution of Sn particulates interference within the lattice as observed in Fig. 5. A more close check at the topography of the 7 g matrix revealed that metallic grain size is dependent on the applied current and potential induced as also affirmed by [7]. Although, the coating propagate in an outgrowth style inform of tips, which is ascribed to the interstitial alteration of $Zn^{2+}$ ion. Hence, the control of the embedded $SnO_2$ particulates within the Zn-rich structure can be linked to the controlled diffusion process through the choice of potential applied. Although [8] mentioned that high current density/potential could lead to unfavorable coating during composite deposition. However, for 13 g alloy matrix of Zn-Al-13Sn-Cl-0.3 V, a good account of the deposits was also observed (Fig. 6). The deposit completely covered the entire surface and further exhibited a coalesced crystallites but not as the former. In essence, diffusion process and the mechanism of the alloy coating is observed to be influenced by composite ions into the nucleus, hence resulting into growing frame under the influence of the applied voltage.

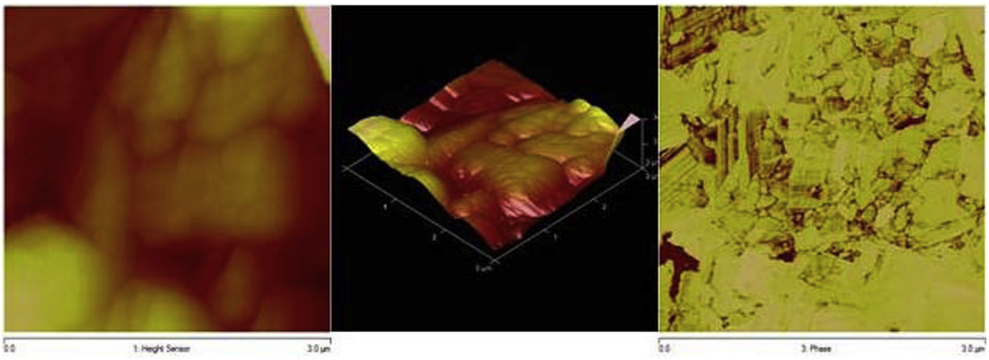

**Fig. 6.** AFM Images of the Zn-Al-13Sn-Cl-0.3 V Film: (a) 2-D image; (b) 3-D Relief Image and (c) Roughness Analysis.

*Solid XRD/Raman analyses of coatings*

The comparison of XRD patterns produced from Zn-Al-$SnO_2$ chloride deposited matrix for Zn-Al-7Sn-Cl-0.3 V and Zn-Al-13Sn-Cl-0.3 V alloys are represented in Figs. 7 and 8 respectively. Sn peaks are seen in the admixed Zn-Al rich bath indicating the adsorption and perfect incorporation of Sn particles into the Zn based matrix. The intermetallic phase containing $Zn_2Al_3Sn$ in the coating had higher peak intensity for Zn-Al-7Sn-Cl-0.3 V over the 13 g deposit observed in Fig. 8. Reason for this could not be really rationalized however; [9] reported that incorporation of larger amount of particle could increase the d-spacing of lattice.

Therefore, with increasing percentage concentration of the $SnO_2$, the diffractive intensity of the Zn-Al based film decreased systematically as observed in Fig. 8 for Zn-Al-13Sn-Cl-0.3 V coating. The prevailing element and phase for Zn-Al-7Sn-Cl-0.3 V composite matrix are Zn, Sn, $Zn_2Al$, AlZnO and $Zn_2Al_3Sn$ as predominant crystal within the deposited system and suggesting an adherent metallic coating.

More so, for Zn-Al-13Sn-Cl-0.3 V composite coating the peak response was moderate but almost merged with Zn intensity. The phase appears with Zn, $Zn_2Sn$, $Zn_2Sn_5Al$ and $Zn_3Sn$. There are few possibilities to this effect as reported by [10] that increasing the tin content in the bath decreased the zinc based content of the alloy deposit which may be due to the stability of the Zn and Al complex thereby forming hexagonal or orthorhombic structure of $Zn_3Sn$.

The Raman pattern also possesses significant peak tracks with doped Sn content. The phase transformations exist significantly with Zn-Al-7Sn-0.3 V within 1500–2900 intensities (see Fig. 9).

*Microstructural study*

The microstructure developed for various Zn-Al-$SnO_2$ alloy composite matrix additions are shown in Figs. 10 and 11. The structure fabricated at 7 g in 0.3 V revealed a reasonable uniform distribution and a small micro particle inter-link around the major metal lattice. The nature of the crystals on the microstructure can be seen to be influenced by the Al-Sn particles migration assisted by the applied potential. Although, there are also slight agglomeration of the composite particles within the interface but a solid interfacial bonding was also observed between the based zinc and the incorporated particles. Comparing these micrographs, with that produced with 13 g Sn induced at 0.5 V, there seems to be de-agglomeration of the particle and more promotion of the movement of particles toward the cathode region leaving the surface with pores (see Fig. 11).

According to [12] the nature of nanocomposite coating produced can be influenced by the concentration of the incorporated particulates and control of process parameter. In its report increase power or potential Increase further the embedment but easy appearance of pores at composite coating interface which is in line with our observation in Fig. 12; hence this caused loose particulate and detachment in Al/Sn. EDS analysis performed on the deposit obtained revealed that the deposit contains zinc, Al and Sn within the entire deposit.

In other to reveal the behaviour of the deposit at lower magnification Fig. 12-13 shows the optical micrographs of the Zn-Al-$SnO_2$ varied particulates. From the results, it can be seen that, the presence of the Al/Sn gave a solid interconnected metallic phase with compact appearance of zinc particulate in white and other admixed layer in black coloured appearances.

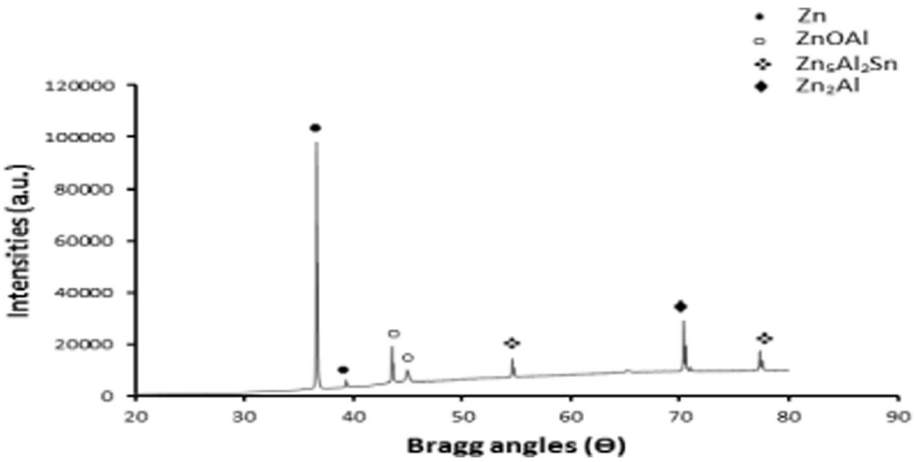


**Fig. 7.** Solid X-ray Diffraction Profile for Zn-Al-7Sn-0.3 V Alloy.

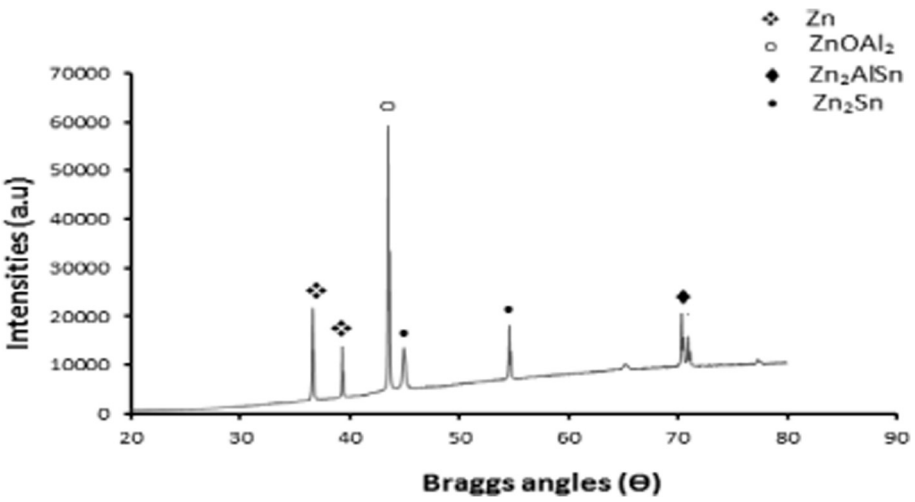


**Fig. 8.** Solid X-ray Diffraction Profile for Zn-Al-13Sn-0.5 V Alloy.

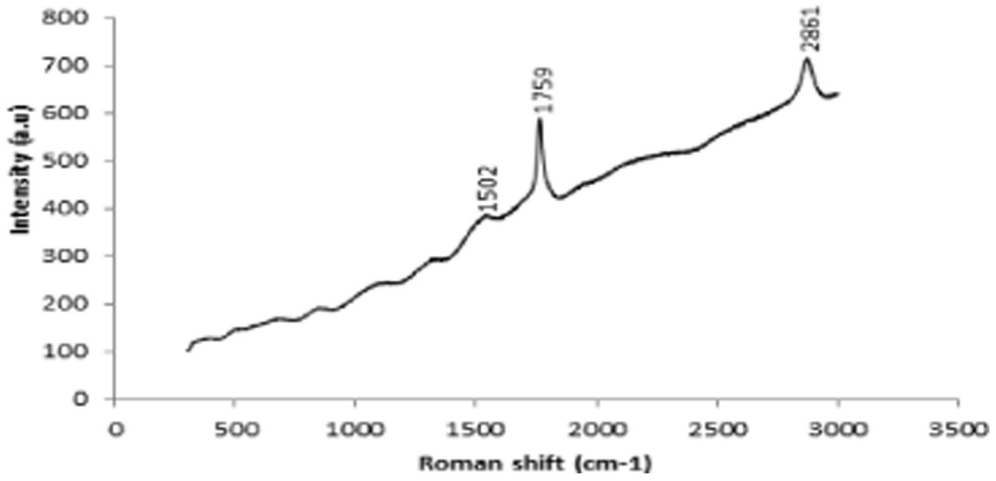


**Fig. 9.** Raman Spectrum for Zn-Al-7Sn-Cl Deposition.

*Mechanical properties*

*Microhardness behaviour of the coatings*

Figs. 14 and 15 represent the hardness properties of $SnO_2$ loading in Zn-Al bath solution and the amount of its varied inclusion in the composite deposit. In general, all composite coatings performed excellently well against the as-received sample. The highest hardness value was obtained with matrix containing 7 g at lower potential coating of 0.3 V (Zn-Al-7Sn-0.3 V-Cl) with 174.8 HVN. The as-received mild steel substrates with initial hardness value of approximately 34 HVN significantly gained improvement geometrically. The combined effort of aluminum and tin was noticed on the zinc matrix to accelerate the strengthening propagation of the composite fabricated coatings. In fact, report by [13] re-affirmed that blending the best properties of two different materials to obtain one material having both desired properties is the major idea of composite coating development. Hence, the fabricated resistance coating hardness obtained is an affirmation to this ideology.

The improvement in hardness was lesser when the composite particle was increased to 13 g at 0.5 V. The decreases in the hardness progression was indeed not expected, reason being that [7] recognized that the increase in particle loading in the bath mostly resulted into amount of particle co-deposited. In other words, loading enhance the possibilities of more particles to get deposited and this may in tune increased the hardness of the composite coating. More so [14] supported the earlier motion that the hardness of the coatings is proportional to the content of particles in the bath but further clarify that increasing current density beyond a certain value is not as significant for particle dispersion into base metal layer. In view of this, the correlation between the current density, potential and the concentration of embedded particle is of significant importance, justifying the reason for decrease in hardness of Zn-Al-7Sn-0.5 V-Cl composite coating. It is evident that at 13 g, particles get agglomerated in the bath. Hence less uniform deposit can be noticed with direct consequence on hardness behaviour. This argument is in line with the report presented by [15]. For Zn-Al-13Sn-0.3 V-Cl composite coating, the hardness is 117.4 HVN as compared to when the deposit was perform on 0.5 V with 13 g. It is evident that the response to improvement is in relation to lower potential used. It is also interesting to note, that the higher amount of particulate incorporated does not connote significant crystallite to support hardness improvement but rather the effect of plating parameters especially the plating potential at lower value [8].

Micrographs of the microhardness indentations of the samples (uncoated and coated) at different process parameter were taken using a high diamond based optical hardness microscope

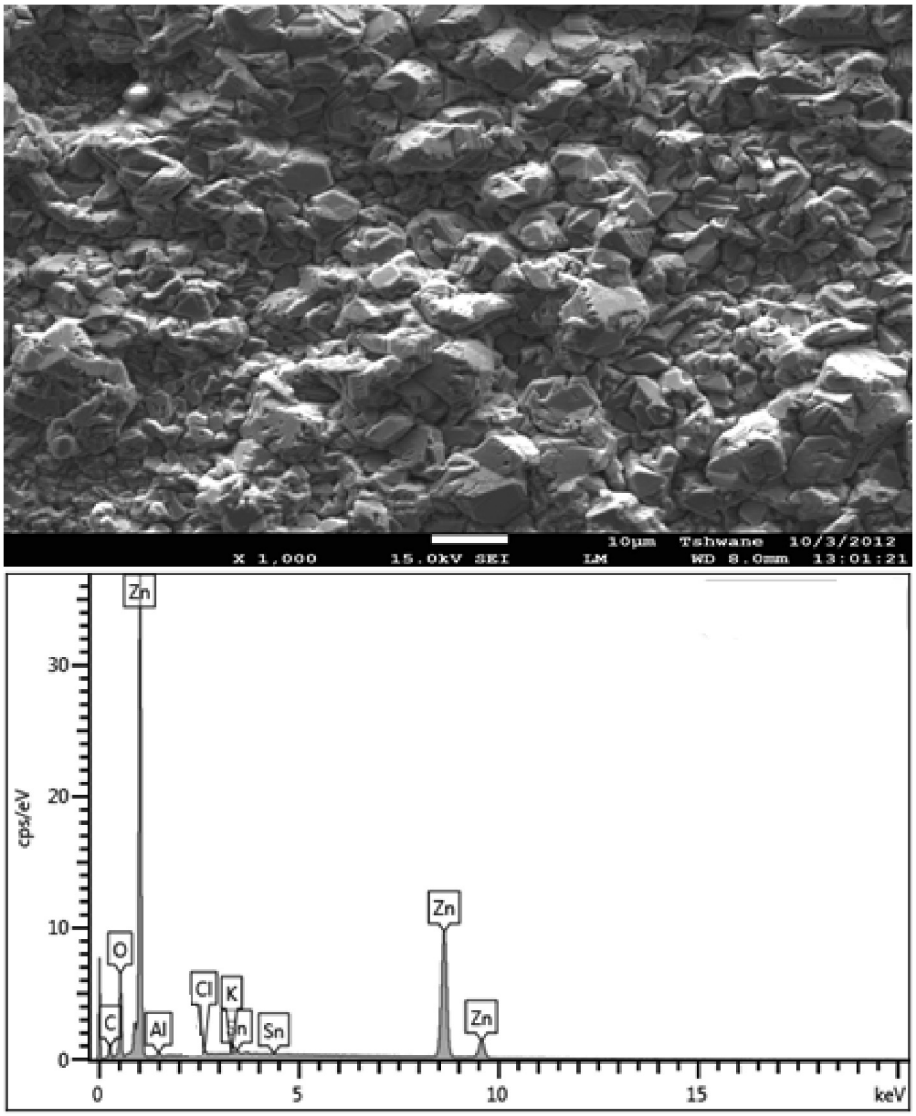


**Fig. 10.** SEM/EDS Spectra showing the Surface Morphology of Zn-Al7Sn-0.3 V Chloride Deposition.

(Fig. 15a–e) to obtain a qualitative evaluation of the hardness properties. From the indentations, different samples clearly show that the particulate intensity reduced with voltage of deposition thereby increasing the microhardness behaviour. More so, the microhardness indentation of the as-received sample was maximally reduced and distorted which feasibly due to the low microhardness characteristics of the samples.

*Wear behaviour of the coatings*

Fig. 16 present the wear plastic deformation trend of deposited alloy composite coating and its comparison with the based metal. From the results observed, the wear resistance attained by composite fabricated coating was remarkable. It is evident that Al/$SnO_2$ strengthening phase lead to the remarkable increase in anti-wear resistance above the as-received sample. Among the produced composite coating samples, the coating processed at Zn-Al-7Sn-0.3 V-Cl and Zn-Al-7Sn-0.5 V-Cl had the highest wear resistance properties. This is largely attributed to the activities of the functional embedded Al/Sn particulate and hence results into changes in microstructure of the coating. The incorporation of this particle helps to retard the progression of dislocation and plastic initiation that may occur. Subsequently for composite fabricated with Zn-Al-13Sn-0.3 V-Cl and Zn-Al-13Sn-0.5 V-Cl the wear loss are slightly higher. A reasonable number of factors might be responsible; such as porosity, adhesion and concentration of introduced particulate as attested by [14]. It is of necessity to mention further that proper diffusion and adsorption of the particulate into the lattice site of base metal is a function of the optimum concentration of the composite-particle. On the contrary, the beneficial effect of Al/Sn particle when used above 7 g at 0.5 V could result into plastic deformation due to fall off.

The friction coefficients of composite coating under non lubricated condition at room temperature are presented in Figs. 17 and 18. As can be seen, the composite coatings exhibited a lower friction coefficient as the time and sliding velocity progresses. In all, the introduction of particulates enable the zinc base metal to possess a better strengthening characteristics which in turn assist in reducing plastic deformation and further provide lower friction coefficient observed. In fact, [16] said solid particles emphasizes the fracture and wear resistance. Invariably, coating resistance tends to increase with embedded particulates and thereby provide lower friction coefficient. The wear scar from the wear mechanism observed for Zn-Al-$SnO_2$ composite coating series is presented in Fig. 19a-c. The deformations were quite severe with dominance

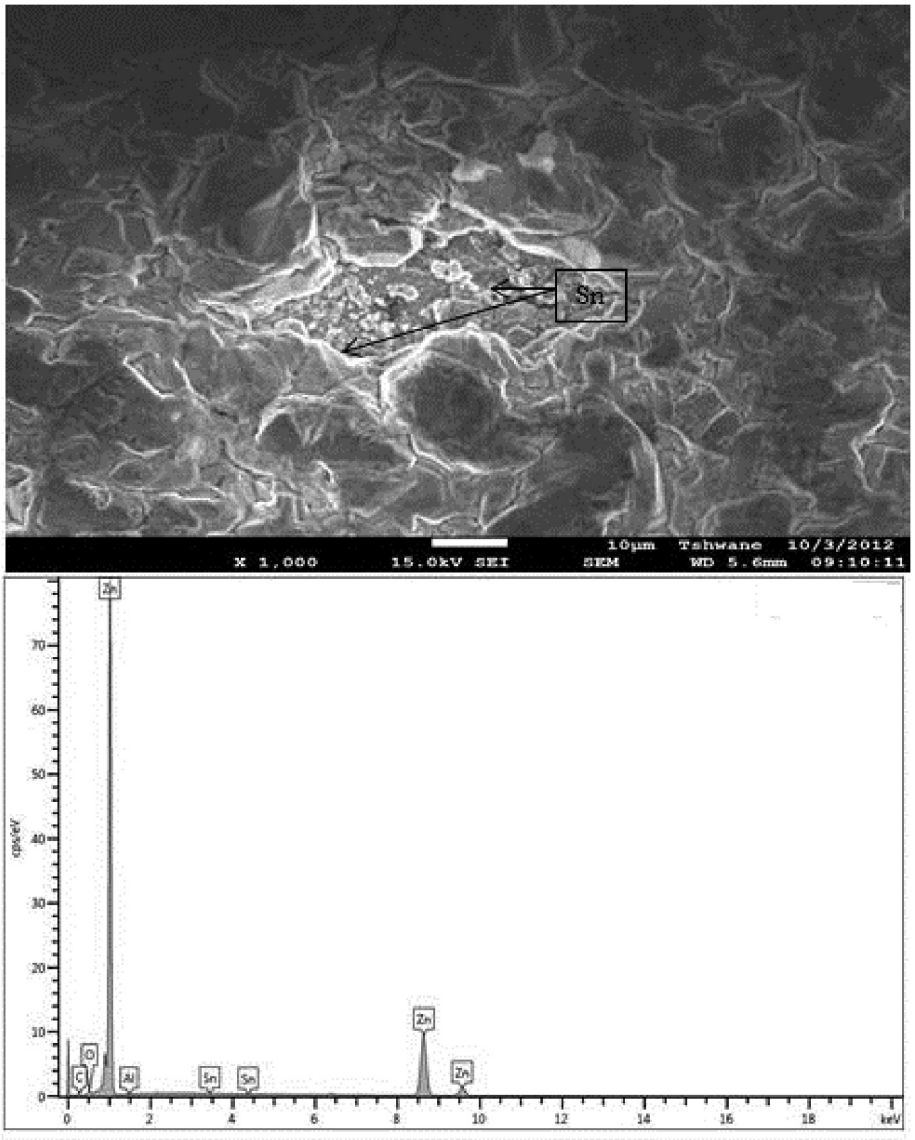


**Fig. 11.** SEM/EDS showing the Surface Morphology of Zn-Al-13Sn-0.5 V Chloride Deposition.

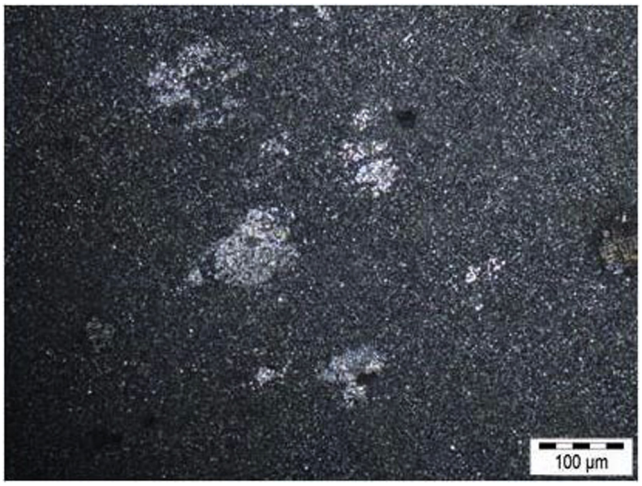


**Fig. 12.** Optical Micrograph of Zn-Al-7Sn-0.3 V Chloride Deposition.

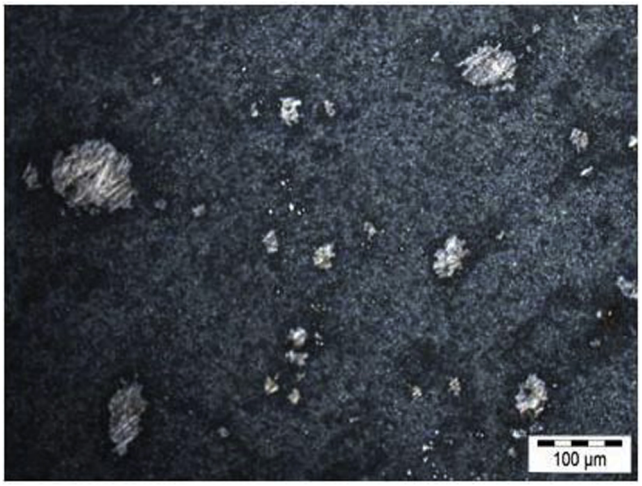


**Fig. 13.** Optical Micrograph of Zn-Al-13Sn-0.5 V Chloride Deposition.

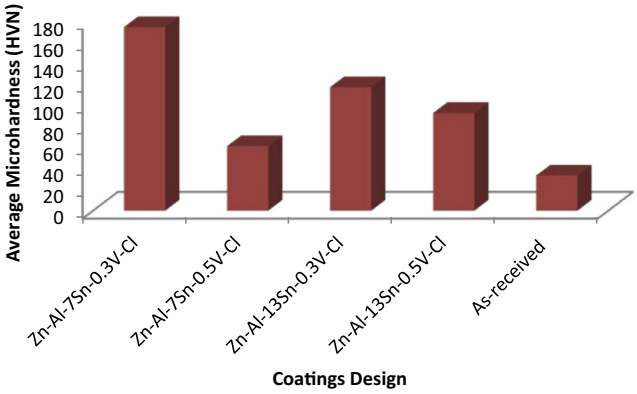


**Fig. 14.** Microhardness Chart for Zn-Al-Sn-Cl Deposition.

of grooves, cracks and severe scratch mark within the surface of the as-received mild steel substrate. The scratches were noticed to be deep in that there are extensive abrasion and easy penetration between the counter body and the surfaces.

For the coated composite (see Fig. 19b, c), along the wear track, slight deformation were notice. Although there seem to be resistible force against the counter body owing to little degree of deformation and scale revolved round at the interface on the coated layers. It should be mentioned that, the anti-wear propagation of the deposited alloy was due to the interference of the composite matrix and the pool of intermetallic phases formed. The bonding characteristics and morphology were seen to justify the resilient effort to wear resistance properties observed.

*Electrochemical behaviour of the coatings*

To know the reactivity and vulnerability of Zn-Al-$SnO_2$ composite coating in 3.65% simulated NaCl environment, linear polarization technique were carried out. Fig. 20 shows the Tafel plots of deposited composite fabricated under different applied potential and varied concentration of additives. As can be seen, all of the corrosion potentials of Zn-Al-$SnO_2$ composite coatings tend toward more positive region than the control sample. This progression implies that there was refusal of the chemical initiation as a result of incorporation of the alpha phase aluminum particle with the help of conjugal interference of $Sn^{2+}$.

However, it is important to mention that the suppression of the cathodic and anodic process by the activities of the admixed composite lower the current density to gain higher corrosion potential recorded. The corrosion potential and current density result were obtained by making use of Tafel slope method by [4,14]. The corrosion current density and potential for as-received sample as tabulated in Table 4 is 7.04E−02 A/cm$^2$ and −1.53900 V respectively; and for the best among the composite coating Zn-Al-7Sn-0.3 V-Cl is 1.40E−05 A/cm$^2$, and −1.05469 V respectively. The least in corrosion resistance among the produced coatings was Zn-Al-7Sn-0.5 V-Cl alloy matrix which also gave significant account of incorporated additive in zinc rich with $E_{corr}$ and $I_{corr}$ of −1.26190 V and

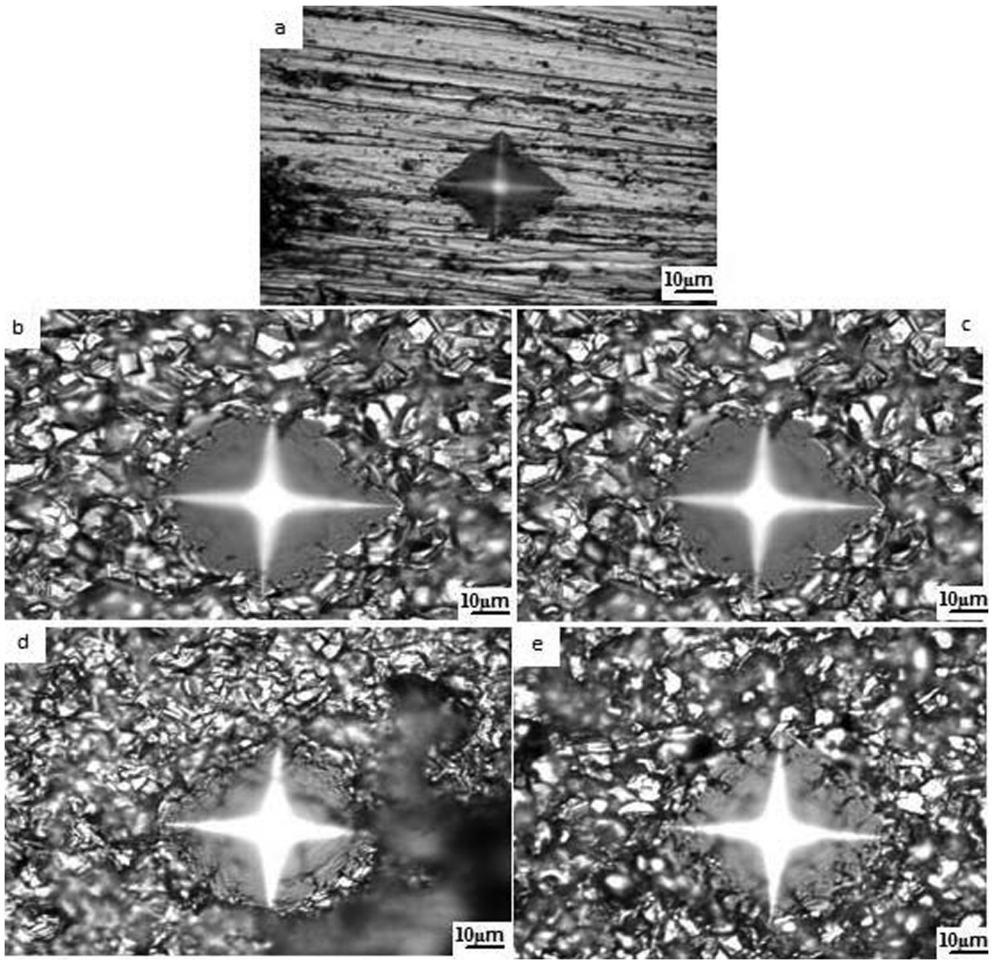


**Fig. 15.** Microhardness indentation micrographs for a) as-received sample b) Zn-Al-7Sn-0.3 V-Cl c) Zn-Al-7Sn-0.5 V-Cl d) Zn-Al-13Sn-0.3 V-Cl e) Zn-Al-13Sn-0.5 V-Cl.

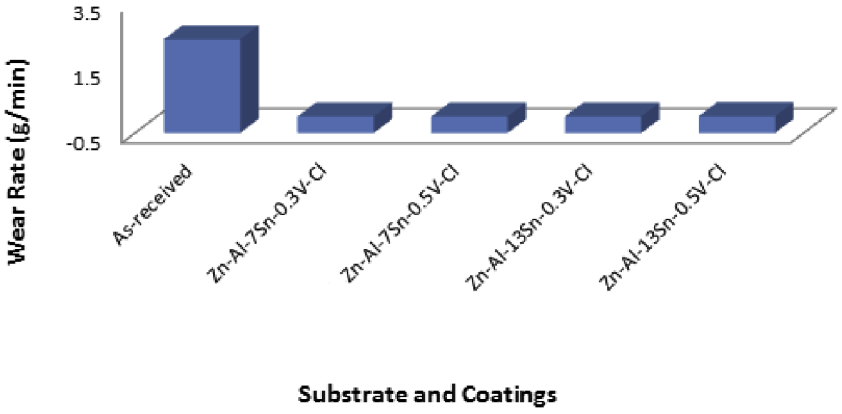


**Fig. 16.** Wear rate of deposited alloys.

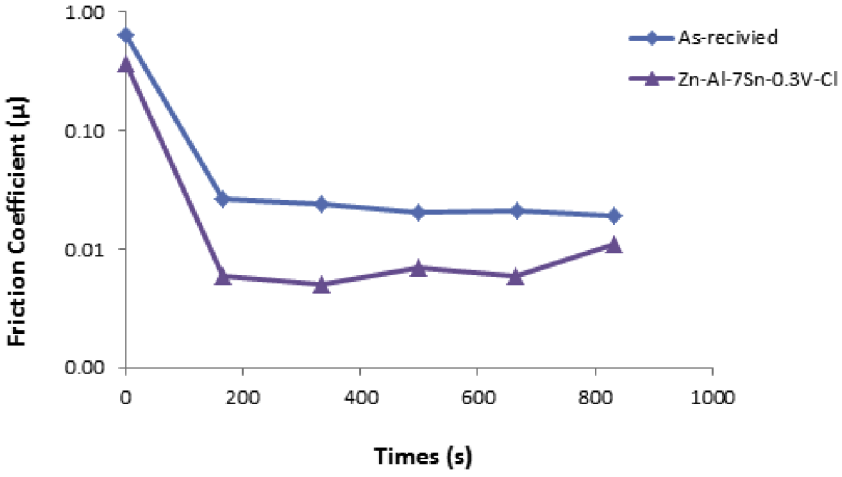


**Fig. 17.** Friction coefficient against time of deposited coating.

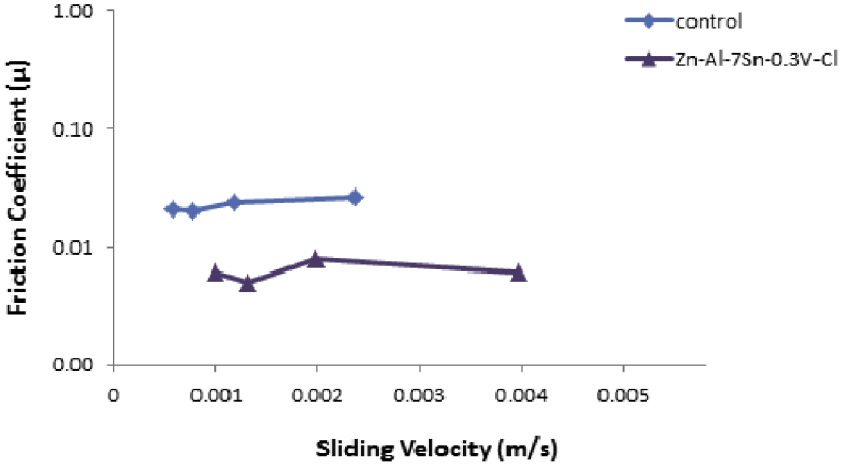


**Fig. 18.** Friction coefficient against sliding velocity of deposited coating.

1.77E−05 A/cm$^2$ respectively, a three time geometric progression of corrosion current resistance compared to the as-received sample.

In all, Zn-Al/$SnO_2$ composite coating possess a better corrosion resistance improvement as their inclusion does not pose any detrimental effect or defects between the metal substrate and the deposited particulate.

The mild steel sample which had high corrosion rate of about 4.1 mm/yr deteriorates aggressively, although this is expected due to lack of surface defense against basic oxide, halide and chloride dissemination. In other words, for the composite coatings Al/$SnO_2$ incorporation, it was noticed to reduce the area for the initiation of anodic dissolution of the Zn alloy coating. In view of this, it can be concluded that the existence of $Al^{3+}$/$Sn^{2+}$ions on mild steel

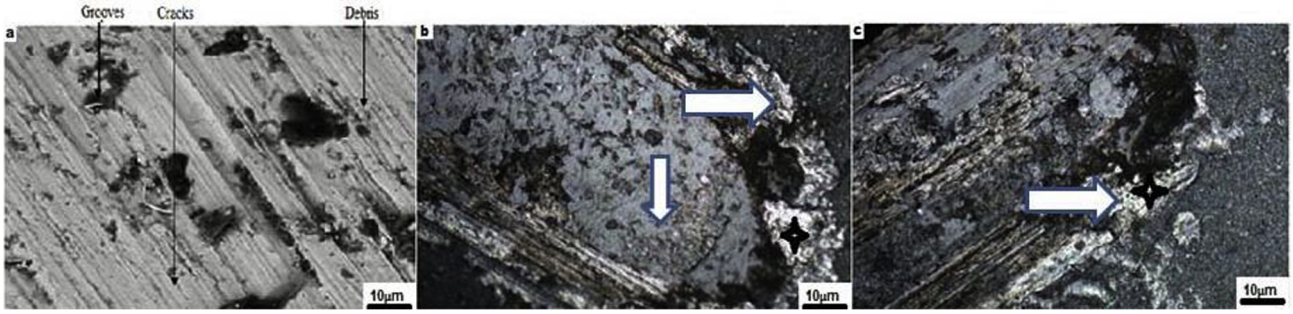


**Fig. 19.** Optical images showing the wear scar effect on microstructures at (a) As-received (b) Zn-Al-7Sn-0.3 V (c) Zn-Al-13Sn-0.3 V.

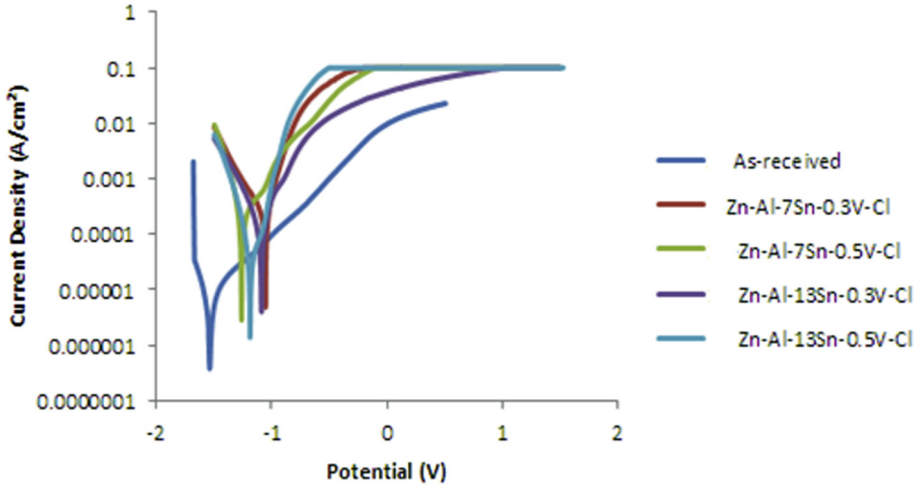


**Fig. 20.** Potentiodynamic Curves for Zn-Al-Sn-Cl Deposition.

**Table 4**
Potentiodynamic Polarization of Deposited Coating.

| Sample | $I_{corr}$ (A/cm$^2$) | $R_P$ (Ω) | $E_{corr}$ (V) | Corrosion Rate (mm/yr) |
|---|---|---|---|---|
| As-received | 7.04E−02 | 2.7600 | −1.53900 | 4.1 |
| Zn-Al-7Sn-0.3 V-Cl | 1.40E−05 | 555.44 | −1.05469 | 0.005837 |
| Zn-Al-7Sn-0.5 V-Cl | 1.77E−05 | 64.603 | −1.26190 | 0.073934 |
| Zn-Al-13Sn-0.3 V-Cl | 1.84E−05 | 371.17 | −1.08826 | 0.007694 |
| Zn-Al-13Sn-0.5 V-Cl | 3.75E−05 | 278.72 | −1.18866 | 0.015627 |

substrate defensed deterioration that might have occurred. The activity and stability of deposited coating after corrosion were observed with the help of atomic force microscope analysis. From all indications, the coating do not suffer from pronounced corrosion attack as a result of the compact adhesion and perfect adsorption bound effect between the incorporated composite fabricated coating (see Figs. 21 and 22) for Zn-Al-7Sn-0.3 V alloy. Interestingly, corrosion resistance can be affected by microstructure and texture which are interconnected to the plating process parameters [16]; in these studies, the structural properties of the Zn-Al-7Sn-0.3 V seem to be in line with this ideology. The situation sounds slightly different with coating obtained with Zn-Al-13Sn-0.5 V alloy.

Invariably the possible formation of iron oxide layer becomes more laudable in the presence of chloride within surface lattices of unprotected mild steel leading to dissolution and the presumed reaction as follows:

$$Fe + H_2O + Cl^- \rightarrow [FeClOH]ads + H^+ + e^- \quad (1)$$

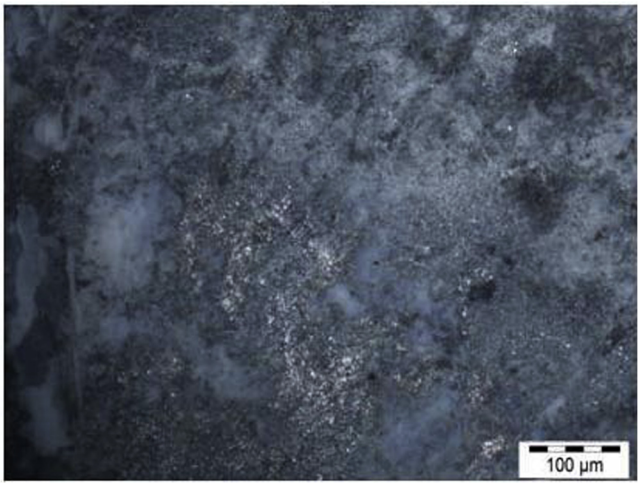


**Fig. 21.** Optical Micrograph of Zn-Al-7Sn-0.3 V Chloride Deposition after Corrosion.

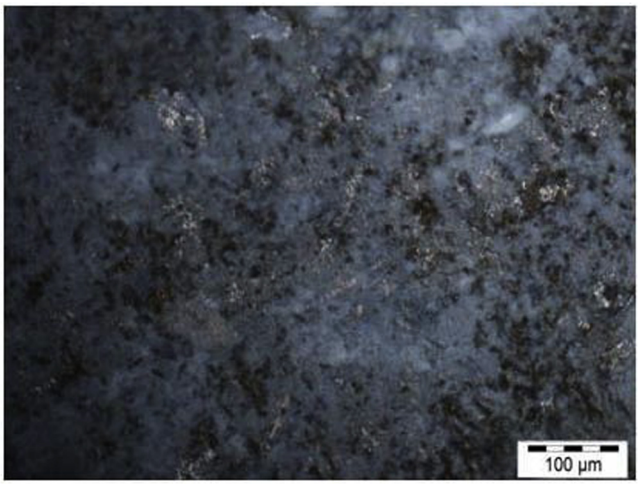


**Fig. 22.** Optical Micrograph of Zn-Al-13Sn-0.3 V Chloride Deposition after Corrosion.

$$[FeClOH] + H^{+} \rightarrow Fe^{2+} + Cl^{-} + H_2O \quad (2)$$

The reaction revealed highly unstable nature of mild steel in the presence of chloride ion and the possible corrosion products.

The coating morphology is affected slightly with Zn-Al-13Sn-0.5 V alloy compared to Zn-Al-7Sn-0.5 V coating; reason for this might be due to the larger particle formed within the interface as a result of number of inclusion, however, instead of forming larger coverage they tend to pull off as the trend of time and current induced progresses. Slight affinity of chloride within the interfacial coverage was observed with few pits.

## Conclusions

Successful electrodeposition of Al/$SnO_2$ composite particulate on zinc containing electrolyte bath was achieved with the following deductions:

- The co-deposition of Zn-Al-$SnO_2$ in the zinc composite coating improved the hardness characteristics of the coatings. The best composite coating with highest hardness properties was prepared under 7 g/L at 0.3 V with Zn-Al-7Sn-0.3 V matrix. The addition of the Al/$SnO_2$ particulate not only distort the coating structure but obviously helped to provide good grain size and well adhered structure.
- The corrosion resistance of mild steel was improved with the strengthening characteristics of the induced particle. A more passive region was obtained from all composite coatings with invariably lower corrosion current density.
- The pitting corrosion attack suffered by Zn-Al-13Sn-0.5 V is attributed to fewer chloride ionic migrations and fallout of agglomerated crystal.
- The anti-wear resistance was visible for all composite coatings fabricated especially with Zn-Al-7Sn-0.3 V alloy posing good lower coefficient of friction and wear mass loss.

## Acknowledgements

This material is based upon work supported financially by the National Research Foundation, South Africa. The equipment support by Surface Engineering Research Centre (SERC) Tshwane University of Technology, Pretoria is deeply appreciated.

## References

[1] Fayomi OSI, Popoola API, Daniyan AA. Hybrid effect of an in-situ multilayer Zn-ZnO-$Cr_2O_3$ electrodeposited nano-composite coatings for extended application Taylor and Francis. Part Sci Technol 2016. http://dx.doi.org/10.1080/02726351.2016.1163305.
[2] Fayomi OSI, Popoola API, Olorunniwo OE. Structural and properties of Zn-Al2O3-SiC nano-composite coatings by direct electrolytic process Springer. Int J Adv Manuf Technol 2016. http://dx.doi.org/10.1007/s00170-016-8428-4.
[3] Fayomi OSI, Popoola API, Loto CA, Adedokun ST. Evaluation of composition, microstructure characterization and interfacial properties of Zn–SnO2 metal matrix composite coating Springer. Prot Met Phys Chem Surf 2016;52(2):238–43.
[4] Lin Z, Li X, Xu L. Electrodeposition and corrosion behavior of zinc-nickel films obtained from acid solutions: effects of TEOS as additive. Int J Electrochem Sci 2012;7:12507–17.
[5] Tiwari SK, Sahu RK, Pramanick AK, Singh R. Development of conversion coating on mild steel prior to sol gel nanostructured $Al_2O_3$ coating for enhancement of corrosion resistance. Surf Coat Tech 2011;205:4960–7.
[6] Guo S, Xu L, Zhang L, Chang W, Lu M. Corrosion of alloy steels containing 2% chromium in $CO_2$ environments. J Corros Sci 2012;63:246–58.
[7] Popoola API, Fayomi OSI, Popoola OM. Comparative studies of microstructural, tribological and corrosion properties of plated Zn and Zn-Alloy coatings. Int J Electrochem Sci 2012;7:4860–70.
[8] Murside H, Mubel A. Effect of electrolyte pH and Cu concentration on microstructure of electrodeposited Ni-Cu alloy films. Surf Coat Technol 2011;206:1430–8.
[9] Yang G, Chai S, Xiong X, Zhang S, Yu L, Zhang P. Preparations and tribological properties of surface modified Cu nanoparticles. Trans Nonferrous Met Soc China 2012;22:366–72.
[10] Vathsala K, Venkatesha TV. Zn-$ZrO_2$ nanocomposition and evaluation of corrosion resistance. J Appl Surf Sci 2011;257:8929–36.
[11] Frade T, Bouzon Z, Gomes A, Da Silva MI, Pereira MI. Pulsed-reverse current electrodeposition of Zn and Zn-TiO2 nanocomposite films. Surf Coat Technol 2010;204:3592.
[12] Zhu X, Cai C, Zheng G, Zhang Z, Li J. Electrodeposition and corrosion behaviour of nanostructured Ni-TiN composite films. Trans Non Ferrous Met Soc China 2011;21:2216–24.
[13] Subramanian B, Mohan S, Jayakrishnan S. Structural, microstructural and corrosion properties of brush plated copper–tin alloy coatings. Surf Coat Technol 2006;201:1145–51.
[14] Dong Z, Peng X, Guan Y, Li L, Wang F. Optimization of composition and structure of electrodeposited Ni-Cr composites for increasing the oxidation resistance. Corros Sci 2012;62:147–52.
[15] Zheng HY, An MZ. Electrodeposition of Zn-Ni-Al2O3 nanocomposite coatings under ultrasound conditions. J Alloys Compd 2008;459:548–52.
[16] Sancakoglu O, Culha O, Toparli M, Agaday B, Celik E. Co-deposited Zn-submicron sized $Al_2O_3$ composite coatings: production, characterization and micromechanical properties. J Mater Design 2011;32:4054–61.
[17] Wang G, Zhu L, Liu H, Li W. Zinc-graphite composite coating for anti-fouling application. J Mater Sci Lett 2011;65:3095–7.
[18] Blejan D, Muresan LM. Corrosion behaviour of Zn-Ni-$Al_2O_3$ NXSAanocomposite coatings obtained by electrodeposition from alkaline electrolytes. Mater Corros 2012;63:1–6.
[19] Hongmark S, Hedenqvist P, Jacobson S. Tribological properties of thin hard coatings: demands and evaluation. J Surf Coat Technol 1997;90:247–57.
[20] Rusu DE, Ispas A, Bund A, Gheorghies C, Cârâc G. Corrosion tests of nickel coatings prepared from a Watts-type bath. J Coat Technol Res 2012;9(1):87–95.
[21] Fayomi OSI, Popoola API, Oloruntoba DT. Nanoparticle dispersion, microstructure and thermal effect of multi-doped ZrO2/SiC from sulphate induced electrolyte Springer. Prot Met Phys Chem Surf 2016;52(3):512–6.
[22] Popoola API, Aigbodion VS, Fayomi OSI. Surface characterization, mechanical properties and corrosion behaviour of ternary based Zn–ZnO–$SiO_2$ composite coating of mild steel. Elsevier. J. Alloys Compd 2016;654:561–6.
[23] Popoola API, Aigbodion VS, Fayomi OSI. Anti-corrosion coating of mild steel using ternary Zn-ZnO-Y2O3 electrodeposition Elsevier. Surf Coat Technol 2016. http://dx.doi.org/10.1016/j.surfcoat.2016.05.018.
[24] Abdulwahab M, Fayomi OSI, Popoola API. Structural evolution, thermomechanical recrystallization and electrochemical corrosion properties of Ni-Cu-Mg amorphous coating on mild steel fabricated by dual-anode electrolytic processing Elsevier. Appl Surf Sci 2016. http://dx.doi.org/10.1016/j.apsusc.2016.03.075.
[25] Fayomi OSI, Popoola API. An investigation of properties of Zn coated mild. Int J Electrochem Sci 2012;7:6555–70.
[26] Jegannathan S, Sankara TSN, Ravichandran K, Rajeswari S. Formation of zinc-zinc phosphate composite coatings by cathodic electrochemical treatment. J Surf Coat Technol 2006;200:4117–26.